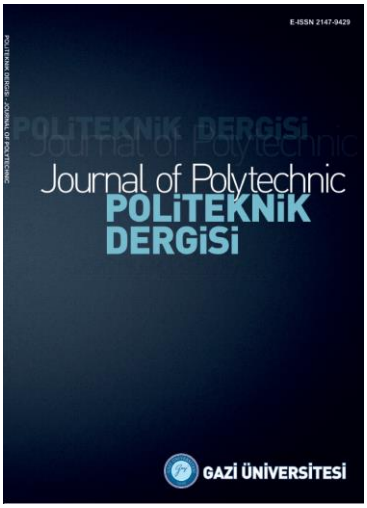

POLİTEKNİK DERGİSİ

JOURNAL of POLYTECHNIC

ISSN: 1302-0900 (PRINT), ISSN: 2147-9429 (ONLINE)
URL: http://dergipark.org.tr/politeknik

Use of friction pendulum system for seismic isolation of museum artifacts: mathematical modeling and parametric study

Müze eserlerinin sismik izolasyonu için sürtünmeli sarkaç sisteminin kullanımı: matematiksel modelleme ve parametrik çalışma

***Yazar(lar) (Author(s))**: Abdullah ÇELİK[1], Cumhur Oktay AZELOĞLU[2]*

ORCID[1]: 0000-0003-4403-2218

ORCID[2]: 0000-0001-5283-9447

To cite to this article: Çelik A. and Azeloğlu C. O., "Use of friction pendulum system for seismic ısolation of museum artifacts: mathematical modeling and parametric study", ***Journal of Polytechnic***, 27(6): 2313-2324, (2024).

Bu makaleye şu şekilde atıfta bulunabilirsiniz: Çelik A. ve Azeloğlu C. O., "Use of friction pendulum system for seismic ısolation of museum artifacts: mathematical modeling and parametric study", ***Politeknik Dergisi***, 27(6): 2313-2324, (2024).

Erişim linki (To link to this article): http://dergipark.org.tr/politeknik/archive

DOI: 10.2339/politeknik.1386758

Use of Friction Pendulum System for Seismic Isolation of Museum Artifacts: Mathematical Modeling and Parametric Study

Highlights

- *Establishing a mathematical model for a museum artifact isolated with the FPS inside of a structure*
- *Carrying out a parametric study involving variations in the values of the effective radius of curvature and the friction coefficient*
- *Investigation of the effectiveness of the FPS by comparing the isolated and non-isolated museum artifact*

Graphical Abstract

In this study, a mathematical model was established for a museum artifact isolated by a single friction pendulum bearing. Afterward, a parametric study was carried out, and the effectiveness of the FPS was analyzed.

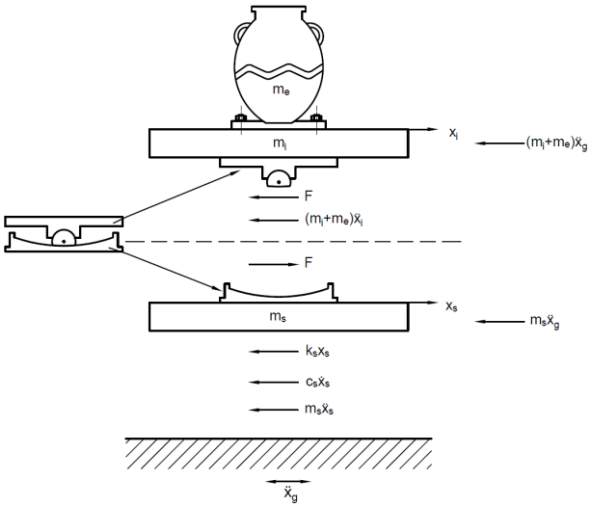

Figure. Free body diagram of the museum artifact isolated by the friction pendulum system

Aim

This study aims to investigate the response of friction pendulum system according to the values of effective radius of curvature and coefficient of friction and to examine their effectiveness in seismic isolation of museum artifacts.

Design & Methodology

The mathematical model developed by Fenz and Constantinou was created for museum artifacts on the first floor. The responses of the isolator are examined for different effective radii of curvatures between 0.5 m and 3 m at 0.025 m intervals, and seven different friction coefficient parameters of the FPS.

Originality

The originality of the study stems from the investigation of the parameters and effectiveness of the single friction pendulum-type bearings for museum artifacts.

Findings

When the isolated and the non-isolated case are compared with the determined fmax= 0.06 and fmin= 0.03, Reff= 3 m parameters: Substantial decreases of 29.47% and 58.56% are noted in both peak and RMS accelerations for the L'Aquila Earthquakes East-West component, along with 25.01% and 51.42% reductions in the North-South direction. Additionally, RMS displacements between the floor and the artifact for both East-West and North-South components are alleviated by 37.23% and 10.88%, while peak displacements exhibit minor rises of 3.25% and 1.10%, respectively.

Conclusion

The simulation results show that the acceleration values of the museum artifact were significantly reduced, while the relative displacement between the floor and the museum artifact was within reasonable limits.

Declaration of Ethical Standards

The author(s) of this article declare that the materials and methods used in this study do not require ethical committee permission and/or legal-special permission.

Use of Friction Pendulum System for Seismic Isolation of Museum Artifacts: Mathematical Modeling and Parametric Study

Araştırma Makalesi / Research Article

Abdullah ÇELİK[1*], C. Oktay AZELOĞLU[1]

[1]Yildiz Technical University, Department of Mechanical Engineering, 34349 Istanbul, Türkiye

(Geliş/Received : 06.11.2023 ; Kabul/Accepted : 20.03.2024 ; Erken Görünüm/Early View : 29.03.2024)

ABSTRACT

Earthquakes seriously threaten precious artifacts in museums worldwide. Many historical pieces of inestimable importance that are considered the common heritage of humanity have been damaged by earthquakes. Robust measures must be put in place to protect museum artifacts from the perils associated with seismic risks. Seismic isolation devices like spherically shaped bearings are one of the best options to prevent seismic damage of museum artifacts thanks to achieving a long period under low weights. Therefore, the objective of this research is to assess the effectiveness of friction pendulum-type isolators, one of the spherically shaped bearings, in seismic isolation of museum artifacts and to identify the appropriate design parameters. In this study, a non-isolated single-degree-of-freedom model and a 2-degree-of-freedom model isolated with a friction pendulum bearing inside a building were established for a museum artifact. A parametric study was conducted using the RMS and the peak accelerations and displacements of the isolated mass at different values of friction coefficient and effective radius of curvature, as well as the maximum displacement of the friction pendulum system. Afterward, the non-isolated and isolated mass responses were compared in the time domain based on selected f_{max}= 0.06 and f_{min}= 0.03, R_{eff} = 3 m parameters obtained from the parametric study. The simulation results demonstrate a substantial reduction in the acceleration values of the museum artifact, while simultaneously maintaining the relative displacement between the floor and the museum artifact within acceptable limits.

Anahtar Kelimeler: Seismic isolation, friction pendulum system, museum artifact.

Müze Eserlerinin Sismik İzolasyonu için Sürtünmeli Sarkaç Sisteminin Kullanımı: Matematiksel Modelleme ve Parametrik Çalışma

ÖZ

Depremler, bütün dünyada müzelerdeki değerli eserleri ciddi şekilde tehdit etmektedir. İnsanlığın ortak mirası olarak kabul edilen paha biçilemez öneme sahip pek çok tarihi eser depremlerden zarar görmüştür. Müze eserlerini sismik risklerle ilgili tehlikelerden korumak için ciddi önlemler alınmalıdır. Küresel şekilli mesnetler gibi sismik izolasyon cihazları, düşük ağırlıklar altında periyodu uzatabilmeleri sayesinde müze eserlerinin sismik etkiler sebebiyle hasar görmesini önlemek için en iyi seçeneklerden biridir. Bu nedenle, bu çalışma küresel şekilli mesnetlerden biri olan sürtünmeli sarkaç tipi izolatörlerin müze eserlerinin sismik izolasyonundaki etkinliğini araştırmayı ve uygun tasarım parametrelerini belirlemeyi amaçlamaktadır. Bu çalışmada, bir müze eseri için izole edilmemiş tek serbestlik dereceli ve bina içinde sürtünmeli sarkaç tipi izolatör ile izole edilmiş iki serbestlik dereceli bir model kurulmuştur. Farklı efektif eğrilik yarıçapı ve sürtünme katsayısı değerleri için izole kütlenin maksimum ve ortalama karekök ivme ve yer değiştirme değerleri ile izolatörün maksimum yer değiştirme değeri için parametrik bir çalışma yapılmıştır. Daha sonra, izole edilmemiş kütlenin ve parametrik çalışma sonunda seçilen f_{max}= 0.06 and f_{min}= 0.03, R_{eff} = 3 m parametrelerine sahip bir izolatörle izole edilen kütlenin tepkileri zaman tanım alanında karşılaştırılmıştır. Simülasyon sonuçları, müze eserinin ivme değerlerinin önemli ölçüde azaldığını; aynı zamanda zemin ile müze eseri arasındaki göreli yer değiştirmenin uygun sınırlar içinde olduğunu göstermektedir.

Keywords: Sismik izolasyon, sürtünmeli sarkaç sistemi, müze eseri.

1. INTRODUCTION

Earthquakes not only damage buildings but also pose a threat to museum artifacts such as busts, sculptures, pillars, vases, pottery, ceramics, and art objects. Due to the dynamic amplification effect, the artefacts in the building are subjected to more earthquake forces than the ground movement [1]. Therefore, a moderate earthquake may not damage the structure but may cause irreversible demolition of artifacts. In some cases, the building may not be destroyed, but the museum artifacts are extremely devastated [2, 3]. For example, two sculptures named "Madonna in trono" and "Sant'Antonio Abate" in the National Museum of Abruzzo [4], art objects at the National Museum of Athens [5], Arkhias' Tombstone in Kahramanmaraş Archaeology Museum shown in Figure 1, were damaged during the L'Aquila Earthquake (Mw

*Sorumlu Yazar (Corresponding Author)
e-posta : abcelik@yildiz.edu.tr

(a) (b) (c)

Figure 1. Images of different statues and art objects failure: (a) Statues collapsed in the L'Aquila Earthquake [4], (b) Overturned art objects in the 1999 Athens (Parnitha) Earthquake [5], (c) Arkhias' Tombstone after 2023 Kahramanmaraş Earthquakes

6.3) in 2009, the 1999 Athens (Parnitha) Earthquake (Mw 6.0), and Kahramanmaraş Earthquakes (Mw 7.7, Mw 7.6) in 2023, respectively.

Traditional methods aimed at increasing strength can be applied to safeguard buildings and non-structural components against the effects of ground motions, but these are usually not possible for museum artifacts. Seismic isolation has been considerably utilized to prevent damage to buildings and non-structural elements like museum artifacts in seismic hazard zones for decades. Seismic isolation is a method for reducing the destructive impact of earthquakes on museum artifacts by separating them from the floor. The seismic effects, like absolute acceleration transmitted to the artifact, can be decreased with devices named seismic isolators. The idea of seismic isolation is that rather than improving the durability of the museum artifact, structural components that have low horizontal stiffness, named seismic isolators, are positioned between the floor and the museum artifact, isolating the sensitive artifact from the horizontal or vertical elements of seismic ground motions.

There are three different techniques for the application of seismic isolation represented in Figure 2: base isolation, artifact isolation, and floor isolation. The initial method, named base isolation [6-9], intends to safeguard the structure and its non-structural parts by separating the building from the foundation. However, because the seismic requirements of the structure and secondary systems can differ, the isolation system's design criteria may not be able to fulfill both requirements [10]. The second approach involves individual seismic isolation of each vulnerable museum artifact. The third technique, known as the raised-floor method, involves the installation of a secondary floor system on the building floor to separate a set of artifacts from the earthquake effects.

There are some research has focused on the seismic protection of lightweight objects like museum artifacts. These investigations presented different kinds of isolation devices, such as rubber bearings [11], sliding bearings [12-16], rolling-based systems [17-20], wire rope isolators [21], spring-viscous damper systems [22], active-control systems [23, 24], and hybrid systems that combined active or semi-active and passive systems [25-27]. According to Lambrou and Constantinou, spherical bearings are the most straightforward method for extending the period under low loads. They used the Friction Pendulum System in their study for computer floors because of its long isolation period, high displacement capacity, and absence of stability issues at low loads [12]. There are also applications of seismic isolation to museum artifacts. For instance, four friction pendulum bearings were installed to isolate the "Hermes of Praxiteles" statue, which is exhibited in the Archaeological Museum of Olympia in Greece [28]. Thus, this study aimed to determine and analyze the optimal parameters of a friction pendulum-type bearing for the seismic isolation of each sensitive piece of museum artifacts in a single-story building, either separately or with a raised floor within the story.

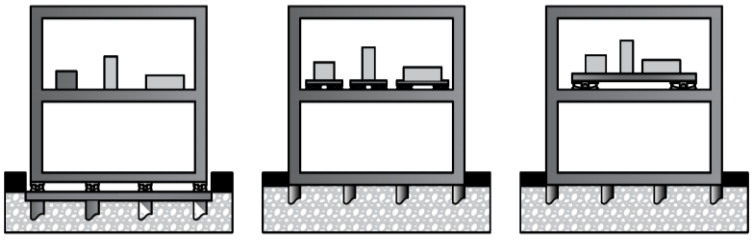

(a) (b) (c)

Figure 2. Schematic illustration of seismic isolation techniques: (a) Base isolation, (b) Artifact isolation, (c) Isolation of artifacts as a group

2. FRICTION PENDULUM SYSTEM

Friction pendulum-type seismic isolation systems are sliding-based bearings in which the restoring force is ensured by their geometry. These systems achieve isolation by utilizing sliding motion and provides damping through the friction generated between the curved surface and the articulated slider. There is no correlation between the flexibility and the energy dissipation of the FPS. This property eases design optimization. Since the FPS behaves like a pendulum, the period of the FPS is not dependent of the weight. It depends on the geometry of the system. This factor holds significant importance in the selection of the FPS for isolating museum artifacts. The period of the friction pendulum system is as follows:

$$T = 2\pi\sqrt{\frac{R}{g}} \tag{1}$$

Herein, R is the radius of the curvature, and g is the gravitational acceleration.

A cross-section view of the friction pendulum-type bearing is given in Figure 3. The FPS comprises of an articulated slider placed on a curved sliding surface, with retainers in place to limit exceeding the capacity of displacement (d) of the sliding surface. The pivot point serves to indicate the specific location around which the slider rotates within the system. The slider height (h) represents the radial distance measured from the concave surface to the pivot point. The friction (μ) between the articulated slider and the sliding surface is velocity-dependent. The FPS maintains its rigidity as long as it stays within the static friction limit. Consequently, it effectively resists the movement when subjected to minor loads.

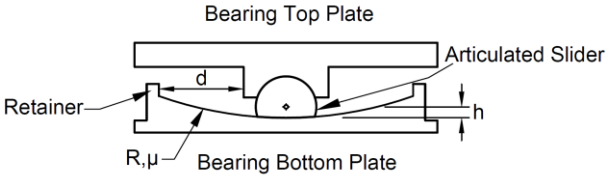

Figure 3. Cross-section of the FPS

The actual period of motion of the isolated system is determined by the effective radius (R_{eff}) of curvature because the vertical and horizontal forces transmitted by the bearing act at the pivot point. In friction pendulum systems, the pivot point can be inside or outside the perimeter defined by the spherical concave surface. The value of the effective radius (R_{eff}) varies according to the position of the pivot point in relation to the surface of the articulated spherical slider. When the pivot point is inside the boundary, the effective radius of curvature (R_{eff}) equals the difference between the radius (R) of the spherical sliding surface and the height (h) of the slider ($R_{eff} = R - h$). Conversely, when the pivot point is located outside this boundary, the effective radius of curvature (R_{eff}) is the sum of the radius (R) and the height (h) of the slider ($R_{eff} = R + h$).

3. MODELING

In the mathematical model for friction pendulum systems developed by Fenz and Constantinou [29, 30], which is used in this study, the velocity-dependent behavior of the coefficient of friction is described as follows:

$$\mu = f_{max} - (f_{max} - f_{min})exp(-a|\dot{x}|) \tag{2}$$

In Equation 2, μ is the velocity-dependent friction coefficient, f_{min} is the nearly zero velocity (static) friction coefficient, f_{max} is the high velocity (dynamic) friction coefficient, a is the ratio parameter controlling the transition between fmin and fmax, $\dot{x}$ is the sliding speed.

The friction pendulum system model includes linear spring elements, where the stiffness relies on the spherical surface's curvature and a friction element with a plasticity determined by a modified Bouc-Wen model. Additionally, a gap element has been incorporated to represent the stiffness behavior of the slider in contact with the restraint. For displacements under a predetermined value, the gap element applies no force. The gap element behaves as a linear spring with significant stiffness beyond this displacement. Therefore, the i^{th} horizontal force (F_i) exerted by the friction pendulum element is as follows:

$$F_i = \frac{W}{R_{effi}}x_i + \mu_i W Z_i + \underbrace{k_r(|x_i| - d_i)sign(x_i)H(|(x_i| - d_i)}_{F_{ri}} \tag{3}$$

In Equation 3, W is the weight (vertical load) on the bearing, R_{effi} is the effective radius of the curvature, x_i is the relative displacement between the slider and the concave surface, μ_i is the velocity-dependent friction coefficient defined in Equation 2, Z_i is the hysteretic coefficient ranging from -1 to 1 defined in Equation 4, the hysteretic coefficient ranging from -1 to 1, F_{ri} is the forces occurring at the contact of the slider with the restraint, k_{ri} is the stiffness of the restraint limiting the displacement, H is the step function, and d_i is the displacement capacity of the ith surface. The equation of the hysteretic variable Z_i is as follows:

$$\frac{dZ_i}{d_t} = \frac{1}{x_{yi}}\{A_i - |Z_i|^{\eta_i}[\gamma_i sign(\dot{x}_i Z_i) + \beta_i]\}\dot{x}_i \tag{4}$$

In Equation 4, x_{yi} is the yield displacement, $\dot{x}$ is the sliding velocity on the given surface; A, η, γ, and β are nondimensional parameters that control the form of the hysteresis loop. Equation 4 and second part of Equation 3 represent friction hysteresis with a continuous function

that approaches pure frictional behavior as x_{yi} approaches zero.

3.1. Non-Isolated Model

In base isolation, since the seismic requirements of the building and the museum artifacts to be isolated may be different, the criteria used for designing the isolation systems may not meet both demands. For this reason, seismic isolation of museum artifacts was done separately within the floor. Since museum artifacts are usually located on the first floor, this model was created for museum artifacts on the first floor. The nonlinear differential equations were solved in the time domain using Matlab/Simulink® [31].

Figure 4 shows the free-body diagram of the non-isolated museum artifact rigidly fixed on the first floor. Here, m_s is the structure of the first-floor structure mass, m_e is the museum artifact mass, k_s is the stiffness of the structure, c_s is the damping of the structure, $\ddot{x}_g$ is the acceleration of the earthquake, x_s, $\dot{x}_s$, and $\ddot{x}_s$ are the displacement, velocity, and acceleration of the museum artifact and the structure, respectively.

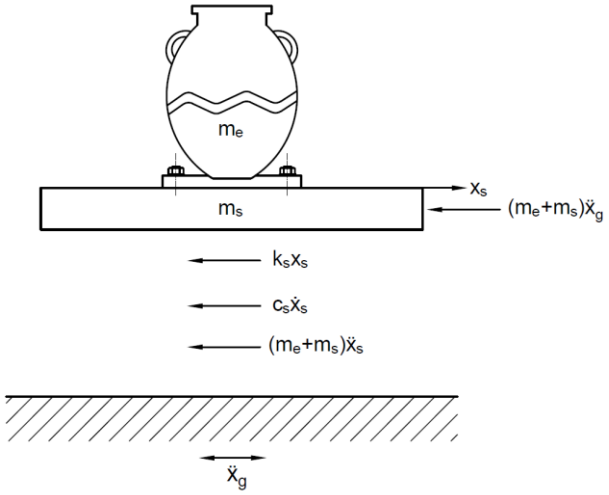

Figure 4. Free-body diagram of the non-isolated museum artifact mass

The equation of motion for the non-isolated museum artifact rigidly connected to the first-floor is obtained as follows:

For first-floor structure mass and museum artifact mass,

$$(m_s + m_e)\ddot{x}_s + k_s x_s + c_s \dot{x}_s = -(m_s + m_e)\ddot{x}_g(t) \quad (5)$$

3.2. The Model Isolated by The Friction Pendulum System

Figure 5 shows the free-body diagram of the museum artifact isolated by a single friction pendulum bearing on the first floor. Herein, m_s is the mass of the first-floor structure and the isolator bottom plate, m_i is the mass of the raised floor and isolator top plate, m_e is the mass of the museum artifact, k_s is the stiffness of the structure and c_s is the damping of the structure. F is the horizontal force due to curvature, $\ddot{x}_g$ is the earthquake acceleration, x_s, $\dot{x}_s$, and $\ddot{x}_s$ are the displacement, velocity, and acceleration of the isolator bottom plate and the structure, respectively; x_i and $\ddot{x}_i$ are the displacement and acceleration of the raised floor, isolator top plate mass and museum artifact, respectively.

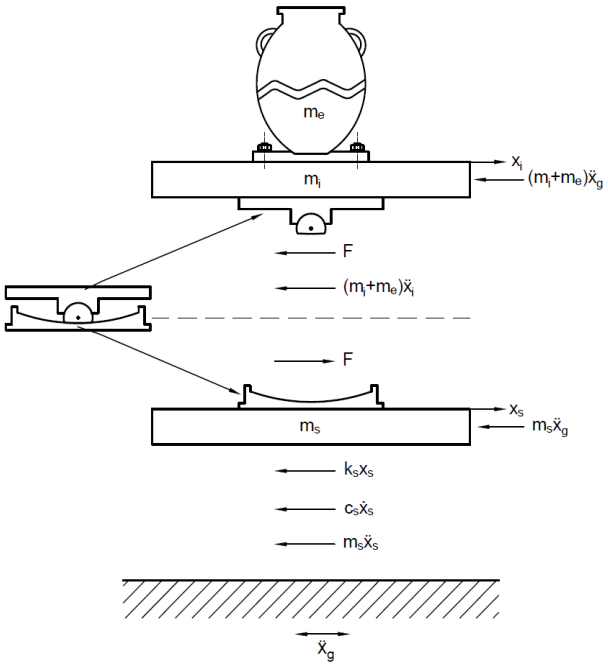

Figure 5. Free body diagram of the museum artifact rigidly attached to the raised floor isolated by the FPS on the structure

The equations of motion of the museum artifact isolated by the FPS on the first-floor are obtained as follows:

For first-floor structure mass and bearing bottom plate mass,

$$m_s\ddot{x}_s + k_s x_s + c_s \dot{x}_s - F = -m_s\ddot{x}_g(t) \quad (6)$$

$$m_s\ddot{x}_s + k_s x_s + c_s \dot{x}_s - \left(\frac{W}{R_{eff}}(x_i - x_s) + \mu WZ + \underbrace{k_r(|(x_i - x_s| - d)sign(x_i - x_s)H(|(x_i - x_s| - d))}_{F_r}\right) = -m_s\ddot{x}_g(t) \quad (7)$$

For bearing top plate, raised floor and museum artifact mass,

$$(m_i + m_e)\ddot{x}_i + F = -(m_i + m_e)\ddot{x}_g(t) \quad (8)$$

$$(m_i + m_e)\ddot{x}_i + (\frac{W}{R_{eff}}(x_i - x_s) + \mu WZ + \underbrace{k_r(|(x_i - x_s| - d)sign(x_i - x_s)H(|(x_i - x_s| - d))}_{\dot{F}_r} = -(m_i + m_e)\ddot{x}_g(t) \quad (9)$$

Velocity dependent coefficient of friction,

$$\mu = f_{max} - (f_{max} - f_{min})exp(-a|\dot{x}_i - \dot{x}_s|) \quad (10)$$

Hysteretic variable,

$$\frac{dZ}{d_t} = \dot{Z} = \frac{1}{x_y}\{A - |Z|^{\eta}[\gamma sign((\dot{x}_i - \dot{x}_s)Z) + \beta]\}(\dot{x}_i - \dot{x}_s) \quad (11)$$

4. PARAMETRIC STUDY

In this section, maximum acceleration, RMS acceleration, maximum displacement, and RMS displacement responses of the museum artifact, and the maximum displacement responses of the isolator for different effective radii of curvature and coefficient of friction parameters of the FPS are obtained and shown on graphs.

4.1. Input Ground Motions

In this study, a well-known non-scaled actual earthquake record due to the damage of museum artifacts, will be used as the input ground motions. This earthquake occurred in a central historic town with a high cultural matter. Museum artifacts like statues were damaged during the earthquake since cultural objects were not seismically protected. The data represents the 2009 L'Aquila Earthquake with a magnitude of M_w 6.3 as recorded at the Centro Valle (AQV) station. East-West and North-South components of the earthquake with maximum ground accelerations of 0.664 g and 0.556 g will be used in the simulations. The acceleration time-history graphs of the earthquake input excitation are illustrated in Figure 6.

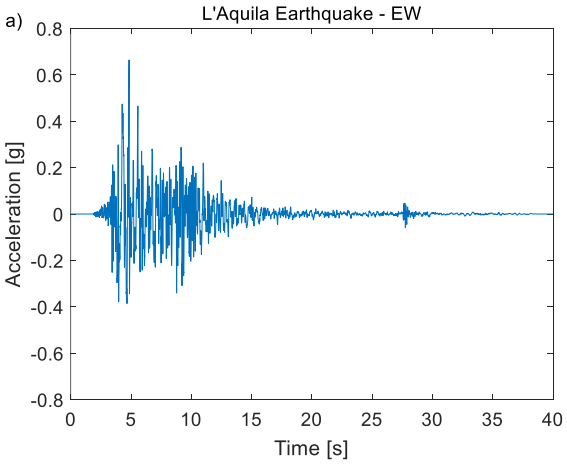

Figure 6. L'Aquila Earthquake ground motion records used for simulations: a) East-West component, b) North-South component

4.2. Effects of Effective Radius and Sliding Coefficient of Friction

In this section, the maximum and RMS acceleration and displacement responses of the museum artifact, and maximum displacement responses of the isolator for different effective radii of curvatures between 0.5 m and 3 m at 0.025 m intervals, and seven different coefficient of friction parameters of the FPS are obtained and shown on graphs.

The first-floor structure properties [32] were taken as mass (m_b)= 450000 kg, damping (c_b)= 26170 Ns/m, and stiffness (k_b)= 18050000 N/m. Museum artifact mass (m_e) is 1000 kg, and the bearing top plate and raised floor mass (m_i) is 250 kg, so the total weight (W) supported by the FPS is 1250 kg. To limit the number of parameters, nearly zero sliding velocity coefficients (f_{min}) is considered twice lower than large velocity sliding coefficients (f_{max}) [33]. Rate parameter (a) was taken as 100 sec/m [31], a commonly used constant value for the FPS. Yield displacement (x_y) is 0.000127 m, and the dimensionless parameters that influence the form of the hysteresis loop: A=1; η =2; γ=0.9; β =0.1 [34].

Simulations are done without retainers because friction pendulum systems have different peak displacements for each effective radius and friction coefficient value. Due to ignoring the retainers, the acceleration results of the isolated mass may be slightly higher, while the displacement results may be slightly lower because of the stiffness behavior that occurs in the contact of the articulated slider with the retainer at the peak displacement of the isolator. Parametric study results will not be affected since retainers are not used for all effective radius and friction coefficient values compared.

Figure 7 to Figure 11 display the peak and RMS acceleration and displacement of the museum artifact isolated with the FPS and these isolators' peak displacements according to different effective radii of

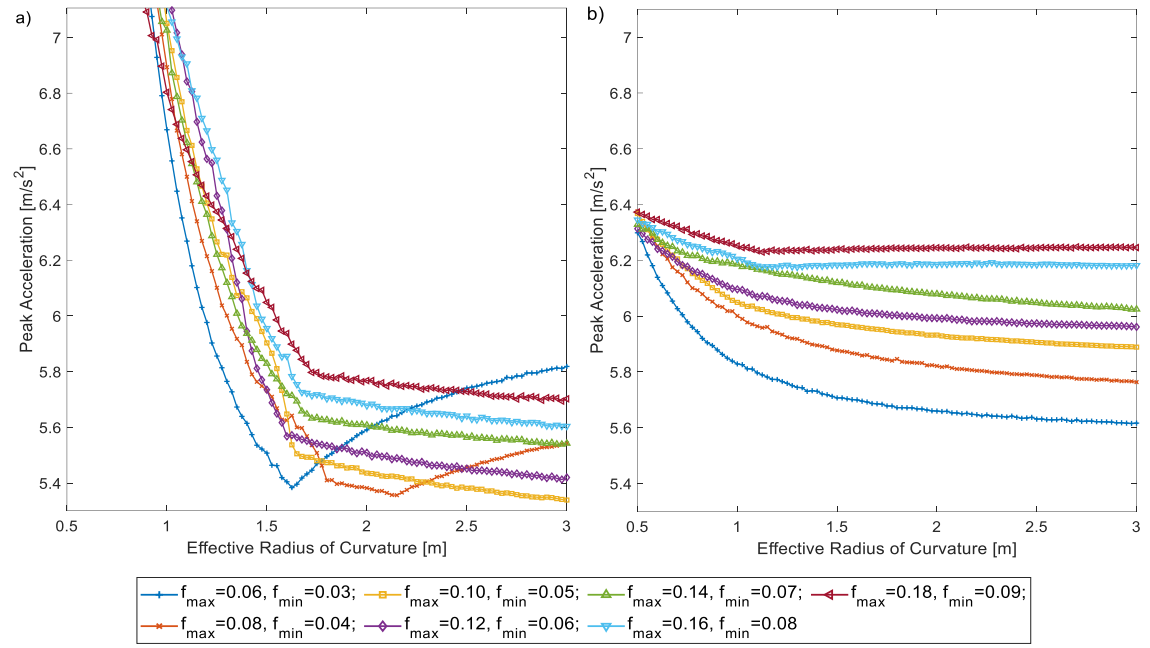

Figure 7. Effects of effective radius and sliding friction coefficients on the peak acceleration of the museum artifact: a) East-West component responses, b) North-South component responses

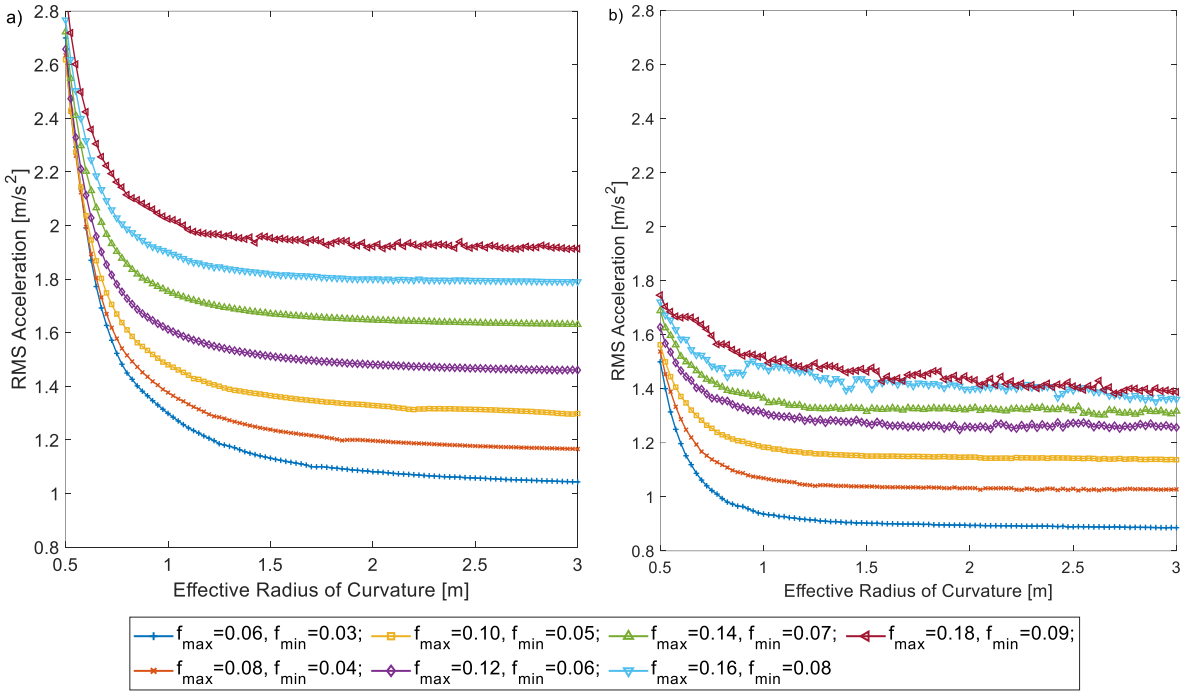

Figure 8. Effects of effective radius and sliding friction coefficients on the RMS acceleration of the museum artifact: a) East-West component responses, b) North-South component responses

curvature and sliding friction coefficients. These graphs indicate the values for every incremental 0.025 m effective radius of curvature of the FPS ranging between 0.5 m and 3 m. The sliding friction coefficients, f_{min} and f_{max}, are considered adaptive to limit the number of design variables. According to this assumption, a nearly zero velocity sliding friction coefficient (f_{min}) is considered twice as lower as a large velocity sliding coefficient of friction (f_{max}). The peak and RMS acceleration and displacement values are shown in figures with seven different adaptive friction coefficients varying from f_{min}: 0.03 to f_{min}: 0.09.

Figure 7 shows the effect of different effective radii of curvature and friction coefficient values of the FPS on the maximum acceleration of the isolated museum artifact obtained using both east-west and north-south components of the L'Aquila Earthquake. When the results of the museum artifact under the influence of the East-West component are analyzed; the minimum peak acceleration value of the museum artifact is 5.3390 m/s^2 for the effective radius of curvature parameter R_{eff} is 3 m,

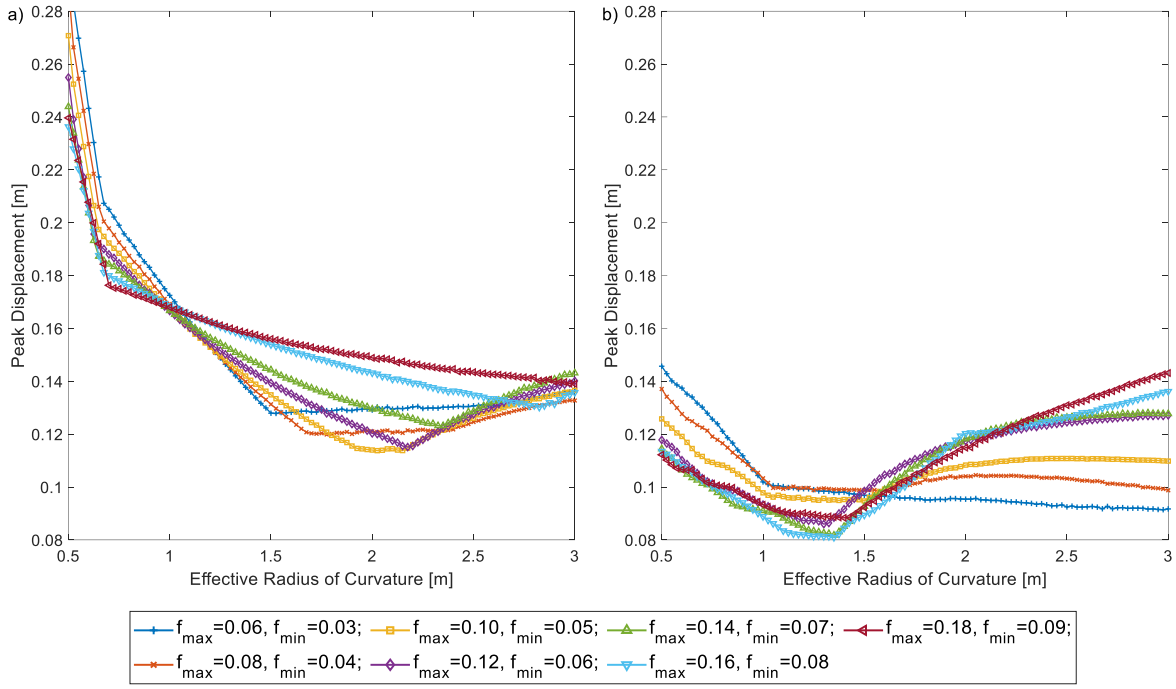

Figure 9. Effects of effective radius and sliding friction coefficients on the peak displacement of the museum artifact: a) East-West component responses, b) North-South component responses

and the friction coefficients f_{max} and f_{min} are 0.10 and 0.05, respectively. Contrary to the responses for other friction coefficients, for the parameters f_{max} = 0.06 and f_{min} = 0.03, the acceleration values of the museum artifact increased after R_{eff} =1.625 m. Similarly, for the parameters f_{max} =0.08 and f_{min} =0.04, the peak acceleration values increased after R_{eff} =2.15m.

In the North-South component results, the lowest peak acceleration is 5.6164 m/s², with $R_{ef\,f}$= 3 m, f_{max} = 0.06, and f_{min} = 0.03 parameters. The observed trend in the North-South component results indicates a decrease in peak acceleration values with a reduction in the friction coefficient but an increase with effective radius values, tending to form a horizontal plateau approximately beyond R_{eff} =1.5 m.

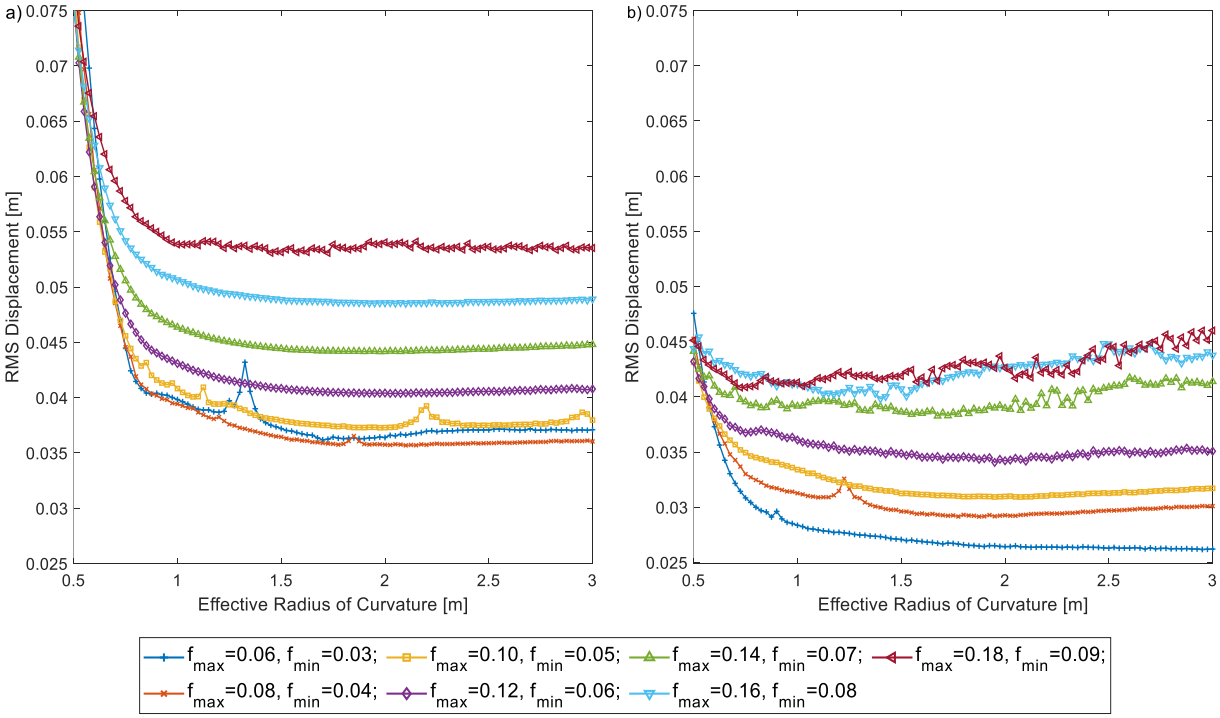

Figure 10. Effects of effective radius and sliding friction coefficients on the RMS displacement of the museum artifact: a) East-West component responses, b) North-South component responses

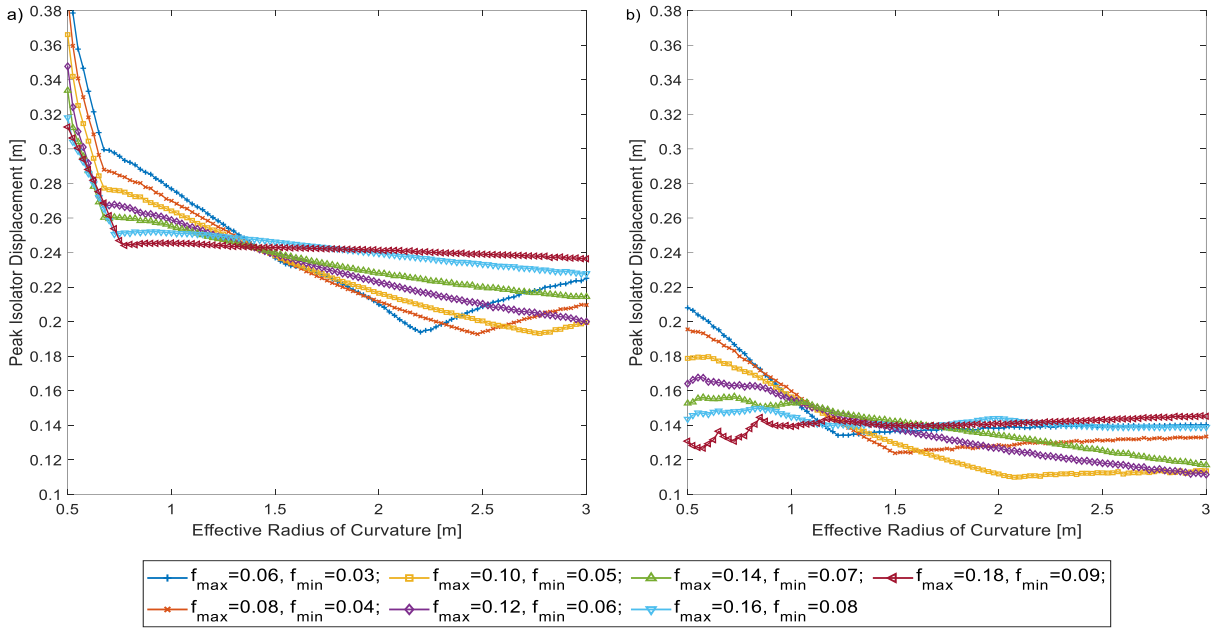

Figure 11. Effects of effective radius and sliding friction coefficients on the peak isolator displacement: a) East-West component responses, b) North-South component responses

According to Figure 8, when analyzing the effects of effective radius and sliding friction coefficients on the RMS acceleration of the isolated mass using the L'Aquila Earthquake input ground motions for both East-West and North-South components, the minimum RMS acceleration value of the museum artifact is 1.0436 m/s^2 and 0.8859 m/s^2 for the effective radius of curvature parameter R_{eff} is 3 m, and the friction coefficients f_{max} and f_{min} are 0.06 and 0.03, respectively. It is observed that as the effective radius of curvature increased, and the sliding friction coefficients decreased, the RMS acceleration values also decreased. RMS acceleration values exhibit a deceleration in their decrease, forming a horizontal plateau approximately beyond R_{eff} =1.5 m in the East-West component and after approximately R_{eff} =1 m in the North-South component. Figure 9 illustrate the effect of different effective radii of curvature and friction coefficient values of the FPS on the maximum displacements between the floor and the museum artifact. While the minimum peak displacement value of the isolated mass for the East-West component is 0.1138 m for the effective radius of curvature parameter R_{eff} is 2.025 m, and the friction coefficients f_{max} is 0.10 and f_{min} is 0.05, the minimum peak displacement of the North-South component is 0.0809 m for R_{eff} = 1.35 m, and f_{max} = 0.16 and f_{min} = 0.08. Isolated masses peak displacements values are within the acceptable limits for all radius and friction coefficient values.

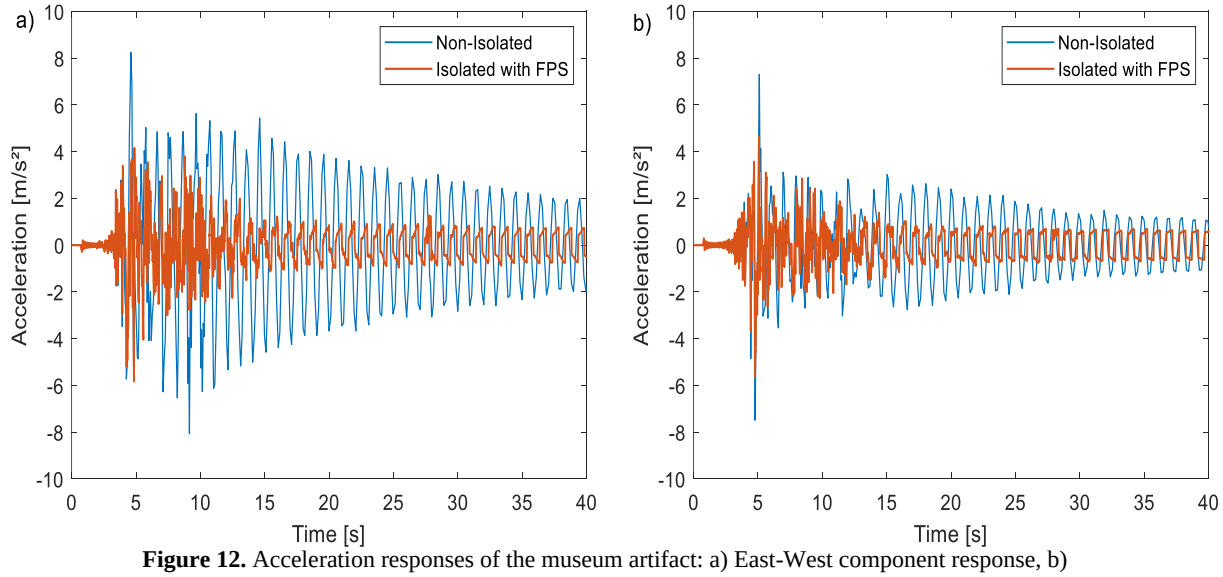

Figure 12. Acceleration responses of the museum artifact: a) East-West component response, b) North-South component response

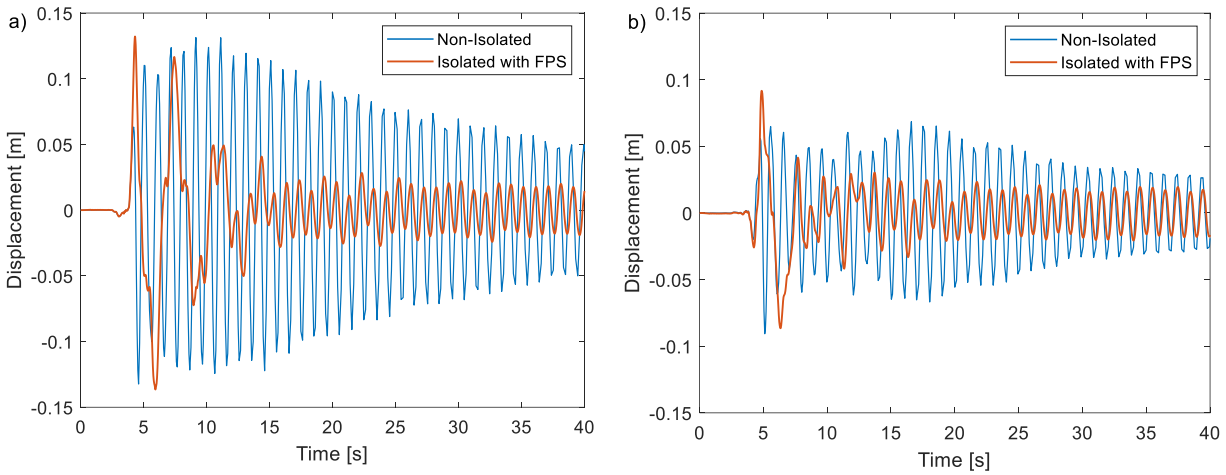

Figure 13. Displacement responses of the museum artifact: a) East-West component response, b) North-South component response

Figure 10 reveals insights into the influence of effective radius and sliding friction coefficients on the RMS displacement between the floor and the museum artifact, as assessed under L'Aquila Earthquake input ground motions. For the East-West component, the minimum RMS displacement of the isolated mass, occurring at an effective radius of curvature R_{eff} = 2.1 m, is 0.0357 m with corresponding friction coefficients f_{max}=0.08 and f_{min} = 0.04. In the North-South component, the minimum RMS displacement is 0.0262 m, observed at R_{eff} = 2.95 m, with friction coefficients f_{max}=0.06 and f_{min}=0.03.

top and bottom plates of the FPS. The East-West component exhibits a minimum peak isolator displacement value of 0.1928 m, observed at an effective radius of curvature R_{eff} = 2.475 m, with friction coefficients f_{max} =0.08 and f_{min} =0.04. Meanwhile, the North-South component demonstrates a minimum peak displacement of 0.1099 m at R_{eff}=2.075 m, with f_{max} =0.10 and f_{min} =0.05. The maximum displacement responses between the top and bottom plates of the FPS remain within reasonable limits across all values of radius and friction coefficients.

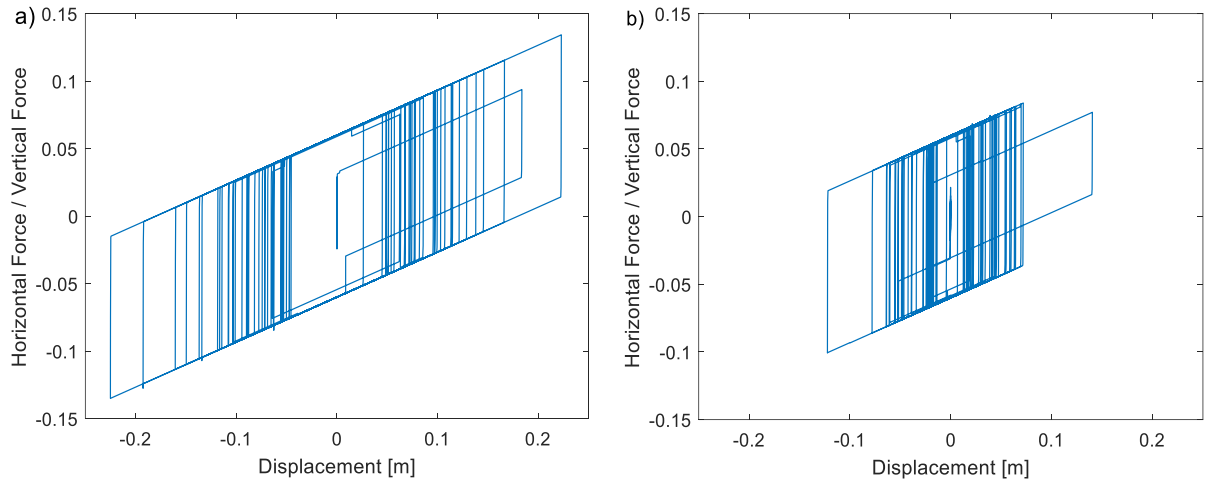

Figure 14. Hysteresis loop of the FPS: a) East-West component response, b) North-South component

While there may be some deviations for both components of the earthquake, it can generally be stated that as the friction coefficient decreases, RMS displacement values tend to decrease. For both components of the earthquake, the decrease in RMS displacement has halted after approximately R_{eff} = 1.5m, and in fact, an increase has been observed, excluding those with friction coefficients f_{max}=0.06 and f_{min}=0.03in the North-South component.
Figure 11 demonstrate the effect of different effective radii of curvature and friction coefficient values of the FPS on maximum displacement responses between the

5. SYSTEM RESPONSES

In this section, the non-isolated and isolated museum artifact responses were simulated using L'Aquila Earthquake ground motions east-west and north-south components. After the parametric study, a performance-oriented selection according to the acceleration of the isolated museum artifact will be made; the specified values for the minimum peak acceleration, f_{max}= 0.06 and f_{min}= 0.03, R_{eff}= 3 m, will be selected to compare to the non-isolated situation. Based on the identified effective radius and friction coefficient values, a displacement

capacity of d=0.23 m has been selected for the compact isolator design, surpassing the peak isolator displacement as indicated by the findings from the parametric study. The retainer stiffness (k_r) is taken as 17500000000 N/m [33] in order to get a very large value. Except for the parameters d, R_{eff}, f_{max} and f_{min}, the same parameters in the parametric study section are also used in this chapter. In order to evaluate the efficiency of the FPS, three responses, the isolated mass acceleration and displacement and the normalized force and bearing displacement relation, will be compared and discussed.

Figure 12 illustrates the isolated and non-isolated acceleration time-history responses of the museum artifact for The L'Aquila Earthquakes East-West and North-South components. When the East-West components response is examined, the peak acceleration value for the museum artifact that is not isolated is 8.2496 m/s^2, the FPS reduced it to 5.8188 m/s^2. The RMS acceleration of non-isolated and isolated with the FPS situations are 2.5182 m/s^2 and 1.0436 m/s^2, respectively. In the evaluation of the North-South components, the non-isolated museum artifact registers a peak acceleration of 7.4871 m/s², while the presence of the FPS mitigates it to 5.6164 m/s². The corresponding RMS acceleration values for the non-isolated and FPS-isolated conditions stand at 1.4001 m/s² and 0.8859 m/s², respectively. The inferences can be made: In the East-West direction, the peak and RMS acceleration values are mitigated by 29.47% and 58.56%, respectively. Similarly, in the North-South direction, the peak and RMS acceleration values experience reductions of 25.01% and 51.42%, respectively. Acceleration values of the isolated mass are substantially minimized compared to the non-isolated situation.

Figure 13 displays the relative displacement between the floor and the museum artifact time-history responses, considering both isolated and non-isolated scenarios, for the East-West and North-South components of the L'Aquila Earthquakes. In analyzing the displacement response of the East-West components, the RMS displacement is reduced from 0.0591 m to 0.0371 m with the implementation of the FPS. The peak displacement in the non-isolated scenario is 0.1323 m, while in the isolated situation, it reaches 0.1366 m. Similarly, for the North-South components of the L'Aquila Earthquakes, the RMS displacement decreases from 0.0294 m to 0.0262 m with the FPS. The peak displacement in the non-isolated situation is 0.0907 m, and in the isolated scenario, it measures 0.0917 m. The deductions drawn from the above observations are as follows: RMS displacement values for the East-West and North-South components of the L'Aquila Earthquakes are mitigated by 37.23% and 10.88%, respectively. However, peak displacements exhibit a very slight increase of 3.25% and 1.10% compared to the non-isolated situation for the respective components. The displacement values fall within acceptable limits for both components during seismic events.

The normalized force and bearing displacement loops of the FPSs under the influence of the East-West and North-South components of the L'Aquila earthquake are shown in Figure 14. In the figures, the horizontal axis shows the relative displacement of the bearing's bottom plate and the top plate of the FPS, while the vertical axis expresses the ratio of the horizontal force acting due to the curvature of the friction surface to the vertical forces from the weight. The initiation of sliding of the FPS starts once the normalized force exceeds the static friction limit on the sliding surface. The period of the motion of the FPS is controlled by the radius of curvature. The FPS devices show nonlinear behavior because of the sliding friction. The force-displacement relation enables information about the amount of energy absorbed. The enclosed areas in Figure 14 depict the dissipated energy by the FPS. According to the hysteresis curves, the maximum value of the ratio of the horizontal forces to the vertical forces are 0.1343 and 0.1008; the maximum displacement of the isolators are 0.2251 m and 0.1404 m for the East-West and North-South components of the L'Aquila earthquake respectively.

6. CONCLUSION

In this study, A mathematical model was established for the museum artifact mounted on a raised floor isolated with a single friction pendulum bearing inside the first floor of a structure. 2009 L'Aquila Earthquakes East-West and North-South components were selected as the input ground motions in the simulations. A parametric study was conducted with variations in the effective radius of curvature and the friction coefficient values. Except for the variations discussed in the parametric study section, it can generally be stated that as the effective radius increases and the friction coefficient decreases, the acceleration values of the museum artifact decrease. The displacement responses remained within reasonable limits across all values of radius and friction coefficients in the parametric study. Later, time history analyses were carried out to compare non-isolated and isolated artifacts using the parameters derived from the parametric study. Significant reductions of 29.47% and 58.56% in peak and RMS accelerations are observed in the East-West component, and 25.01% and 51.42% in the North-South direction, respectively. Furthermore, relative RMS displacements between the floor and the museum artifact for the East-West and North-South components of the L'Aquila Earthquakes are mitigated by 37.23% and 10.88%, while the relative peak displacements show slight increases of 3.25% and 1.10%, respectively. The simulation results demonstrate that the acceleration values of the museum artifact were reduced significantly; meanwhile, the relative displacement between the floor and the museum artifact was within appropriate limits.

ABBREVIATIONS

FPS Friction Pendulum System

RMS Root Mean Square

DECLARATION OF ETHICAL STANDARDS

The authors of this article declare that the materials and methods used in this study do not require ethical committee permission and/or legal-special permission.

AUTHORS' CONTRIBUTIONS

Abdullah ÇELİK: Investigation, modeling, performing simulations, writing.

Cumhur Oktay AZELOĞLU: Supervision, modeling, review & editing.

CONFLICT OF INTEREST

There is no conflict of interest in this study.

REFERENCES

[1] A. E. Zaghi, E. M. Maragakis, A. Itani, and E. Goodwin, "Experimental and analytical studies of hospital piping assemblies subjected to seismic loading," ***Earthq. Spectra***, 28(1): 367–384, (2012).

[2] M. Fragiadakis et al./ ***Arco Conference 2020 Procedings*** / Firenze, Italia, (2020).

[3] Çibuk, K., Gölcük, R. "17 Ağustos 1999 Marmara Depreminin Kocaeli Müzesi'ne Etkileri," ***UNIMUSEUM***, 3(1): 1-14, (2020).

[4] F. Parisi and N. Augenti, "Earthquake damages to cultural heritage constructions and simplified assessment of artworks," ***Eng. Fail. Anal.***, 34: 735–760, (2013).

[5] C. C. Spyrakos, C. A. Maniatakis, and I. M. Taflampas, "Assessment of seismic risk for museum artifacts," ***14th World Conf. Earthq. Eng. - WCEE***, (2008).

[6] F. Naeim and J. M. Kelly, "Design of Seismic Isolated Structures: From Theory to Practice," ***Earthq. Spectra***, 16(3): (1999).

[7] A. Mert, Ş. Gürsoy, Z.Ş. Garip, "Zemin kat yüksekliği ve kat adedi farklı olan betonarme binalarda sismik izolatör kullanımının bina davranışına etkisinin incelenmesi," ***Uluslararası Mühendislik Araştırma ve Geliştirme Dergisi***, 15(2): 671-688, (2023).

[8] E. Alasaf, H. Öztürk, "Sismik izolatörlü yapıların tasarımına etki eden faktörlerin incelenmesi," ***Düzce Üniversitesi Bilim ve Teknoloji Dergisi***, 10(4): 2155-2164, (2022).

[9] N. Güneş, Z. Ç. Ulucan, "Farklı tasarlanmış iki sismik yalıtımlı binanın karşılaştırılması," ***Fırat Üniversitesi Mühendislik Bilimleri Dergisi***, 32(1): 37-46, (2020).

[10] M. Dolce and D. Cardone, "Seismic protection of light secondary systems through different base isolation systems," ***J. Earthq. Eng.***, 7(2): 223–250, (2003).

[11] A. Reggio and M. De Angelis, "Combined primary-secondary system approach to the design of an equipment isolation system with High-Damping Rubber Bearings," ***J. Sound Vib.***, 333(9): 2386–2403, (2014).

[12] V. Lambrou, M. C. Constantinou, "Study of seismic isolation systems for computer floors," Technical Report ***NCEER-94-0020***, May, (1994).

[13] O. R. Jaiswal and S. K. Jain, "Optimum design of resilient sliding isolation system to protect equipments," ***13 th World Conference on Earthquake Engineering***, 78(11): 74–76, (2004).

[14] L. Y. Lu, T. Y. Lee, S. Y. Juang, and S. W. Yeh, "Polynomial friction pendulum isolators (PFPIs) for building floor isolation: An experimental and theoretical study," ***Eng. Struct.***, 56: 970–982, (2013).

[15] S. W. Kim, B. G. Jeon, D. W. Yun, W. Y. Jung, and B. S. Ju, "Seismic experimental assessment of remote terminal unit system with friction pendulum under triaxial shake table tests," ***Metals (Basel)***, 11(9): (2021).

[16] A. Celik, C. O. Azeloglu, "Seismic Isolation of Equipment and Artifacts with Sliding-Based Systems: A Review," ***GLOBCER'22***, 370-379, (2022).

[17] L. Guerreiro, J. Azevedo, and A. H. Muhr, "Seismic tests and numerical modeling of a rolling-ball isolation system," ***J. Earthq. Eng.***, 11(1): 49–66, (2007).

[18] M. Ismail, J. Rodellar, and F. Ikhouane, "An innovative isolation bearing for motion-sensitive equipment," ***J. Sound Vib.***, 326(3-5): 503–521, (2009).

[19] P. S. Harvey and H. P. Gavin, "The nonholonomic and chaotic nature of a rolling isolation system," ***J. Sound Vib.***, 332(14): 3535–3551, (2013).

[20] P. S. Harvey and H. P. Gavin, "Double rolling isolation systems: A mathematical model and experimental validation," ***Int. J. Non. Linear. Mech.***, 61: 80–92, (2014).

[21] G. F. Demetriades, M. C. Constantinou, and A. M. Reinhorn, "Study of wire rope systems for seismic protection of equipment in buildings," Technical Report ***NCEER-92-0012***, (1992).

[22] F. Mezghani, A. Fernandez del Rincón, P. Garcia Fernandez, A. de-Juan, J. Sanchez-Espiga, and F. Viadero Rueda, "Effectiveness study of wire mesh vibration damper for sensitive equipment protection from seismic events," ***Mech. Syst. Signal Process.***, 164, (2022).

[23] M. S. M.E. Talbott, "Active isolation for seismic protection of operating rooms," Technical Report NCEER-90-0010, (1990).

[24] I. Venanzi, L. Ierimonti, and A. L. Materazzi, "Active Base Isolation of Museum Artifacts under Seismic Excitation," ***J. Earthq. Eng.***, 24(3): 506–527, (2020).

[25] J. Y. and P.-Y. L. Yu-Cheng Fan, Chin-Hsiung Loh, "Experimental performance evaluation of an equipment isolation using MR Dampers," ***Earthq. Engng Struct. Dyn.***, 056: 1–6, (2009).

[26] L. Y. Lu and G. L. Lin, "A theoretical study on piezoelectric smart isolation system for seismic protection of equipment in near-fault areas," ***J. Intell. Mater. Syst. Struct.***, 20(2): 217–232, (2009).

[27] H. Salehi, "Application of Robust-Optimum Algorithms in Semi-Active Control Strategy for Seismic Protection of Equipment," in ***15th World Conference on Earthquake Engineering (15WCEE)***, (2012).

[28] A. M. Reinhorn and S. Viti, "Monumental buildings used as museums: Protection or danger for the artifacts?," ***Procedia Struct. Integr.***, 29(2019): 40–47, (2020).

[29] D. M. Fenz and M. C. Constantinou, "Mechanical Behavior of Multi-Spherical Sliding Bearings," Tech. Rep. ***MCEER-08-0007***, (2008).

[30] Fenz and M. C. Constantinou, "Development, implementation and verification of dynamic analysis models for multi-spherical sliding bearings : Technical Report ***MCEER-08-0018***," New York, (2008).

[31] MathWorks. MATLAB and Simulink (R2021b). Natick, ***MA: MathWorks***.

[32] H. Yazıcı, "Çok Serbestlik Dereceli Bir Yapının Titreşimlerinin Bulanık Mantıkla Kontrolü," M. S. thesis, ***Yıldız Technical University,*** Istanbul, (2006).

[33] H. Moeindarbari and T. Taghikhany, "Seismic optimum design of triple friction pendulum bearing subjected to near-fault pulse-like ground motions," ***Struct. Multidiscip. Optim.***, 50(4): 701–716, (2014).

[34] M. Constantinou, A. Mokha, "Teflon Bearings in Base Isolation II: Modeling," ***J. Struct. Eng.,*** 455-474, (1990).